Protein Rebinding to a Surface-Confined Imprint

*Decha Dechtrirat, Katharina J. Jetzschmann, Walter F. M. Stöcklein, Frieder W. Scheller, and Nenad Gajovic-Eichelmann**

A novel strategy to prepare a selective ultrathin molecularly imprinted polymer (MIP) film directly on the gold-based transducer surface for the peptide and protein detection in aqueous solution is demonstrated using a combination of epitope- and electrochemical surface imprinting approach. The synthetic peptide derived from the surface-exposed C-terminus of cytochrome c (Cyt c, residues 96–104) is selected as the template for the imprinting. It is labeled with a fluorescent dye in order to quantitatively evaluate all stages of the imprinting process in terms of changes in mean fluorescence intensity. The labeled peptide template is first chemisorbed on the gold surface as an oriented submonolayer through an additional C-terminal cysteine. After electropolymerization, the template is stripped off electrochemically. To allow the imprinted sites to be confined to the surface, the film thickness is controlled to be comparable to the thickness of the peptide layer. This is achieved by the electropolymerization of scopoletin. Recognition capabilities of the films are characterized and the resulting MIP film is able to selectively capture the template peptide and the corresponding target protein. In case of the peptide recognition, the MIP film can discriminate even the single amino acid mismatched sequences of the target peptide.

1. Introduction

Molecular recognition is a key principle in biology and bioanalysis. Fully synthetic molecularly imprinted polymers (MIPs) pioneered by the groups of Wulff, Shea, and Mosbach[1–3] offer an alternative to biological recognition elements due to their improved stability, effective cost, and rapid fabrication. MIPs are synthetic materials which are prepared by the polymerization in the presence of the template molecule in which the template is embedded within the polymer matrix followed by removal of the template from the polymer. After the template is removed, the remaining cavities complementary to the template in size, shape, and orientation of functionalities are left behind and are capable to selectively recognize the target molecule. Over the past 20 years, a number of application areas of MIPs have been established for low molecular weight compounds.[4] The development of MIPs for proteins, however, is still a great challenge[5–12] due to their large size, high surface complexity, and conformational flexibility. To enable sufficient accessibility for the large target molecules, the imprinted binding sites should be generated at the surface by using the so-called surface imprinting techniques.[13–18]

In analogy to the recognition of antigens by the immune system, selected surface regions of the protein should be addressed for the interaction with the functional groups of the MIP. Following this concept, "epitope imprinting" has been successfully introduced for protein binding MIPs[19–23] in which only a small peptide fragment called epitope rather than the whole protein is templated. Since only this small part of the entire molecule is responsible for the recognition, it is used as a template to imprint the capture sites. To facilitate access of the target protein to the imprinted sites, Nishino et al. have proposed a combination of epitope- and surface imprinting.[24] While the recognition properties of their MIP films are impressive, the integration with transducers is not straightforward, as the resulting MIP film must be peeled off and mounted upside-down onto the transducer. Moreover, the high film thickness of 0.5 mm prevents its use of many common transducers such as SPR, QCM, or amperometric electrodes.

In recent years, fluorescence imaging has undergone a revolution due to the availability of well established fluorescence labeling protocols and highly developed fluorescence microscopes. Fluorescence imaging has attracted interest in the bioanalytical field since it is very sensitive, quantifiable, and non-invasive, and its sample preparation procedure is straightforward as compared to other imaging techniques. Recently, it proved to be a powerful tool to characterize and quantify all the process steps that lead to molecularly imprinted materials, especially when surface imprinting or electrochemical imprinting is concerned.[16,25,26]

Most of the previous reports on MIPs have employed chemical polymerization to prepare these functional materials. Besides this classical means, electropolymerization offers the ability to fine-tune the film thickness and morphology by controlling the charge and deposition mode, and to deposit a film directly at a precise area on the transducer surface even in aqueous electrolyte solution. These superior features of electrochemical polymerization have been successfully applied for the

D. Dechtrirat, K. J. Jetzschmann, Dr. W. F. M. Stöcklein, Prof. F. W. Scheller, Dr. N. Gajovic-Eichelmann
Fraunhofer Institute for Biomedical Engineering
Am Mühlenberg 13, 14476 Golm, Germany
E-mail: Nenad.Gajovic@ibmt.fraunhofer.de

DOI: 10.1002/adfm.201201328

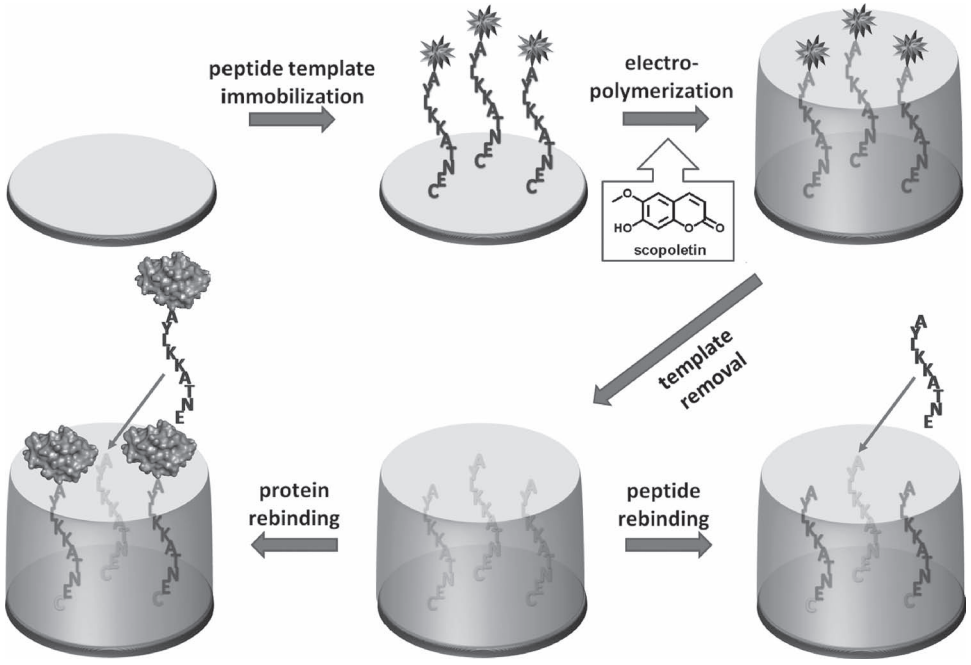

Scheme 1. Schematic representation of the epitope-oriented surface imprinting approach for preparation of MIP ultrathin films.

preparation of high affinity and selectivity MIP films as sensing elements.[27,28]

Herein we present a novel procedure (**Scheme 1**) in which an ultrathin MIP layer can be produced on a planar gold surface by only three simple steps: i) the template peptide is site specifically chemisorbed via an additional C-terminal cysteine on the gold surface forming a submonomolecular coverage; ii) an ultrathin film of the thickness of the target peptide is formed by electropolymerization; and iii) by electrochemically stripping of the peptide, the imprinted binding sites get accessible for the analyte from the solvent phase. For a small molecule, a similar procedure has been proposed by Luo et al.[29] for the imprinting of thiol-modified pyrene. The rebinding was characterized by measuring the access of a redox probe to the electrode surface. We demonstrate that fluorescence imaging is feasible as all the steps in this study including the immobilization and removal of the template peptide, as well as the rebinding of the labeled target peptide and protein can be simply visualized (Figure S1, Supporting Information) and quantified (Table S1, Supporting Information).

To prove this concept, cytochrome c (Cyt c) from bovine heart was chosen as a model protein. The surface-exposed C-terminus peptide containing 9 amino acids (residues 96–104 of Cyt c, AYLKKATNE) was selected as the template because this region has fewer interactions with the other parts of the protein and should be accessible to the binding site of the synthetic receptor. The nonapeptide was considered as the minimum length required for recognition of the protein.[24]

2. Results and Discussion

The formation of a self-assembled monolayer on gold of the cysteine-terminated peptide yields a uniform template orientation via a vectorial gold-thiol interaction. In addition, the template immobilization also improves imprinting efficiency by reducing the conformational space and the thermodynamic motion of the template in the solution.[30] The adsorption of the thiolated template on the gold surface (**Figure 1**, inset) has reached its equilibrium after ca. 3 h, while the concentration dependence (Figure 1) shows saturation at ca. 0.1 mM. The template concentration of 0.05 mM, which results in ca. 60% of the surface coverage, was chosen aiming to maintain the optimal binding capacity of the resulting MIPs.

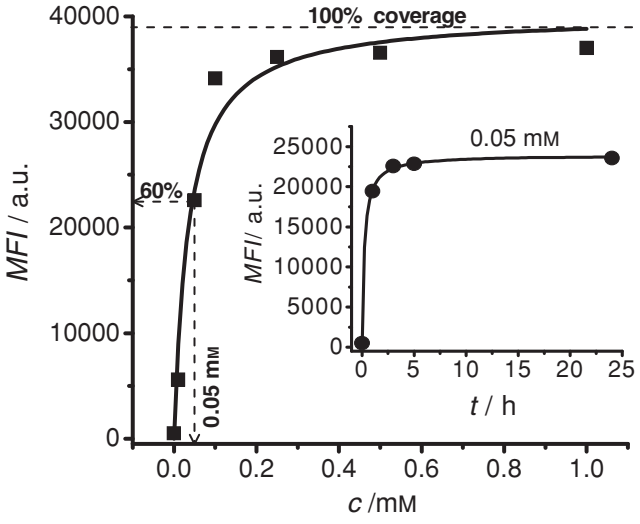

Figure 1. Mean fluorescence intensity (MFI) of TAMRA labeled peptide template chemisorbed on gold surface versus concentration of peptide template in solution. The inset shows the adsorption kinetics.

Table 1. Dependence of percentage of template removal on the number of pulses during electropolymerization, and the film thickness.

No. of pulses	Film thickness[a)] [nm]	% Template removal
1	≈4	≈80
2	≈6	≈40
3	≈7	≈30

[a)]Estimated by SPR.

Table 2. Thickness of the imprinted and non-imprinted film measured by SPR and AFM.

Film	Film thickness [nm]	
	by SPR	by AFM
MIP	≈4	≈3
NIP	≈5	≈4

In the present work, a non-conductive hydrophilic scopoletin based electropolymer (Figure S2, Supporting Information) pioneered by our group[31] was chosen because it can be deposited from dilute aqueous solutions at low oxidation potentials (0.4–0.7 V vs. Ag/AgCl). Under such conditions, the electrochemical stripping of the thiol group of the template is negligible. In addition, this material offers functional groups which are able to form hydrogen bonds, van der Waals forces, and hydrophobic interactions with the template.[32]

After the electrodeposition of poly(scopoletin), the chemisorbed peptide template was removed by electrochemical oxidation of the thiol in combination with a washing step leaving the complementary imprinted cavities in the film. Decrease in fluorescence intensity after the template removal step was used to calculate the percentage of template removal (see Table S1, Supporting Information).

A key step of this approach is to control the thickness of the film to match approximately the length of the peptide. In order to prepare such nanometer thin films, the potential pulse method[33] was applied. By holding the potential of each pulse at 0.7 V for 5 s while varying the number of pulses, thin films with different thicknesses as characterized by using SPR (Figure S3, Supporting Information) were attained. As summarized in **Table 1**, the film with the thickness of ca. 4 nm obtained by applying one potential pulse seems to fit well with the thickness of the peptide layer (in assumption that the peptide is fully stretched). This can be confirmed by the subsequent template removal step in which roughly 80% of the template was removed. As the number of pulses increased, the percentage of the template removal dramatically decreased, revealing that the film was too thick so that the peptide was entrapped within the polymer.

The thickness of the film was confirmed by atomic force microscopy (AFM). This was achieved by scanning a relatively short cantilever (Nano World, Arrow NC) in a contact mode with the applied force of 15 nN over an area of 1×1 μm^2 in order to ablate the deposited polymer layer from the gold surface. As a control, the cantilever was scanned over the bare gold surface to ensure that the same force (15 nN) applied to remove the film could not damage the gold layer. A tapping mode with a much smaller damping force of 2 nN was used to scan over the area of 5×5 μm^2 of the film containing the ablated area in the middle and the resulting topographical AFM images were depicted in Figure S4 (Supporting Information). The line profiles obtained from the cross sectional analysis along the blue line marked in the AFM images represent the surface height features across those points. The relative height changes between the ablated area and the non-ablated film surface were determined as the film thickness. 6500–9000 datapoints from the AFM image measured values available for each individual measurement depending on the exact size of the ablated area. These values were plotted as height histograms and fitted with a 3-parameter Gaussian function (data not shown). As calculated, the thickness of the MIP film was ca. 3 nm, while the thickness of the NIP film was ca. 4 nm. As summarized in **Table 2**, these results were in good agreement with the thicknesses obtained from the SPR measurement. The root mean square (RMS) surface roughness of 2.55 and 2.60 were obtained for the MIP and the NIP film, respectively. No significant distinction of the surface roughness of both films was observed, indicating that surface morphologies of the MIP and the NIP film are nearly the same.

The peptide-depleted film was interacted with different concentrations of Dy-633 labeled peptide. The adsorption isotherms were constructed by plotting the mean fluorescence intensity (MFI) against the bulk concentration, assuming that the latter was in large excess relative to the binding sites (**Figure 2**a). As depicted, the imprinted film clearly shows higher fluorescence for the target peptide as compared with the non-imprinted polymer (NIP) which is formed in the absence of the target peptide and only exhibits low nonspecific binding. At saturation concentration, a tenfold higher binding capacity to the imprinted layer is found, i.e. the imprinting factor of 10 was achieved in this work which is among the greatest values reported so far for peptide MIPs.[20] In the next step, the rebinding of Dy-633 labeled Cyt c was investigated (Figure 2b). The generation of the fluorescence after the interaction with labeled Cyt c shows that the protein can bind to the imprinted film. The imprinted film reveals a sixfold higher binding capacity in respect to the non-imprinted control, i.e., an imprinting factor of 6.

To gain more quantitative information, the data were evaluated in the form of a Scatchard plot (Figure 2a,b, insets) in which the dissociation constants (K_d) of 8.54 and 2.51 μM for Cyt c and the template peptide were obtained, respectively.[34] As compared to our result, Nishino has reported a lower K_d (72.3 nM) for the Cyt c rebinding.[24] It should be, however, noted that two monomers (acrylamide and ethylenebisacrylamide) with higher numbers of hydrogen bonding donor/acceptor sites were used in his case and the cumulative effect of many hydrogen bonds is known to increase the affinity.

Apart from the evaluation of K_d, the Scatchard analysis also provides an insight into the binding sites heterogeneity. Systems which have one type of binding site will exhibit a linear Scatchard plot[35] as it is demonstrated for our imprinted film by the direct site specific immobilization through the thiol-gold interaction.

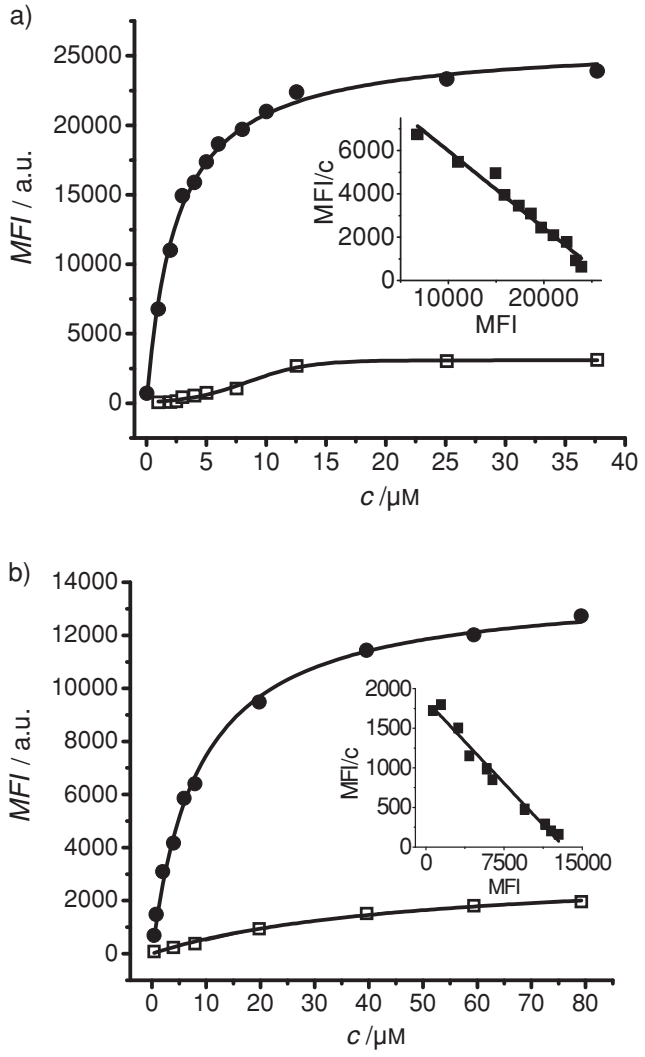

Figure 2. Binding isotherms of a) labeled peptide template and b) labeled Cyt c to the MIP (solid circles) or NIP film (open squares). The insets show the Scatchard plot for the evaluation of K_d.

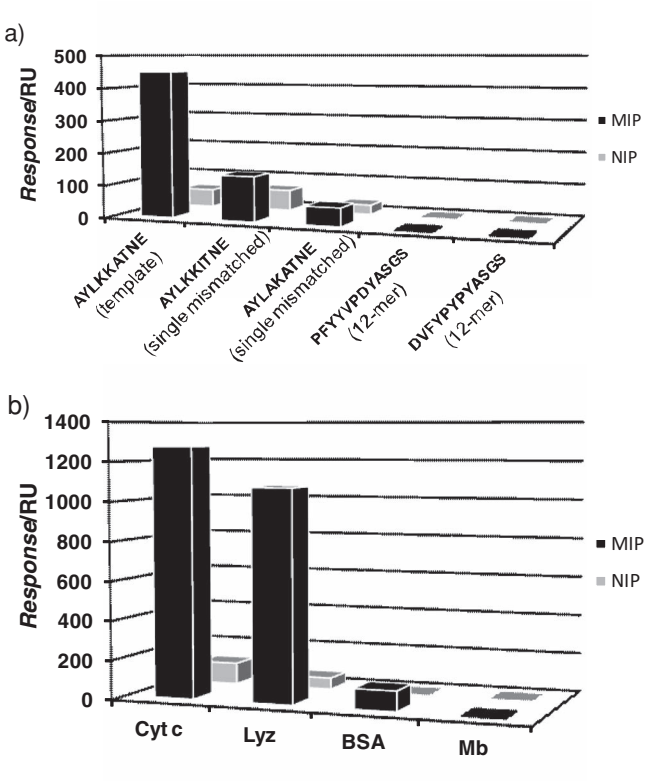

Figure 3. SPR response of MIP and NIP films for a) peptides at 100 μg mL^{-1} and b) proteins at 50 μg mL^{-1}.

Furthermore binding of the imprinted film toward the peptide template (**Figure 3**a) and Cyt c (Figure 3b) was investigated by using the label-free SPR measurements. Using SPR, binding events are monitored in real time avoiding potential bias that may be due to the binding of the fluorophores. Binding of analytes to the sensor surface will cause responses which are proportional to the bound mass of the analytes. As shown, the NIP film exhibits low SPR response which clearly indicates that polyscopoletin itself has low non-specific interaction to the peptides and proteins.

In these experiments two single amino acid mismatched template analogues (i.e., AYLKKITNE, AYLAKATNE) and two non-related peptide sequences (i.e., PFYYVPDYASGS, DVFYPYPYASGS) were used as the control peptides. As depicted in Figure 3a, the template peptide revealed the highest SPR response followed by its single mismatched sequences, while the other non-related peptide sequences yielded almost no response. It is obvious that approximately 90% of residues of the single amino mismatched peptide sequences, namely AYLKKITNE and AYLAKATNE, are identical to the template peptide. However, these responses are three- and eightfold lower than that obtained from the template peptide, indicating that the MIP film can differentiate between the single amino acid mutants and the target peptide.

As characterized by the Zeta potential measurement (data not shown), both of the MIP and NIP films have negatively charged surfaces, but the MIP film is considerably more negative than the NIP film. The higher non-specific binding for the basic peptides (i.e., peptide template and its analogues) to the NIP film is hence supported by electrostatic interactions. Although the electrostatic interaction plays a role during the peptide rebinding, the higher binding capacity of the MIP film to the basic peptide template cannot arise from only the charge interactions but rather mainly through the imprinting as clearly confirmed by the selectivity in peptide recognition.

While the measurements show that Cyt c can bind to the imprinted film, it does not definitively prove that Cyt c can bind to the MIP film via its C-terminus. To prove that Cyt c shares the same binding site with the peptide template, the label-free SPR experiments in a competitive format are performed. This was done by monitoring the real-time binding between the imprinted film and the aqueous solutions of Cyt c, template peptide, and a pre-mixture containing Cyt c/template peptide. Since the response in SPR is directly proportional to the molecular weight of the bound analyte and Cyt c is larger than the

peptide template, the sensor signal obtained from Cyt c is obviously higher than that obtained from the peptide as depicted in **Figure 4**a. When the same amount of Cyt c is mixed with the same amount of peptide, the observed SPR response is lower than Cyt c but higher than the peptide indicating that Cyt c and the peptide compete with each other in order to occupy the same binding pocket. This can also imply that Cyt c is recognized by the MIP film through its C-terminus. Since Cyt c forms a compact globular structure in its native state, binding of the protein to the imprinted film via its C-terminus could happen only when this part is partially unfolded.

Previous theoretical and experimental studies have suggested that native Cyt c could be converted into a C-terminal open-ended structure by partial dissociation of its C-terminus from the rest part of the protein.[36–38] These results might be transferred to the binding of Cyt c to the imprinted film. In analogy to the cardiolipin-induced unfolding, when positively charged Cyt c has reached the negatively charged surface of the imprinted film, the electrostatic interactions have taken place and caused the C-terminal end of this protein to fray. Once the tail has unfolded, it will penetrate into imprinted site and will be stabilized through multivalent interactions (i.e., hydrogen bonds, van der Waals forces, and hydrophobic interactions) between the C-terminus sequence and its complementary pre-oriented functional groups within the polymer domain yielding to specific recognition. In contrast to the imprinted film, the NIP film contains no imprinted site. Hence, the specific binding through the imprinting effect should not be observed. The non-specific binding to the NIP film rather stems from the charge interaction. Since the electrostatic interactions play a key role in the induced unfolding mechanism of the C-terminus of Cyt c, disrupting this force by increasing the ionic strength of the buffer (i.e., increasing salt concentration) could inhibit the rebinding of Cyt c to the MIP film. This would be confirmed as the concentration of NaCl in the rebinding buffer was increased to 1 M, no binding of Cyt c was observed (data not shown).

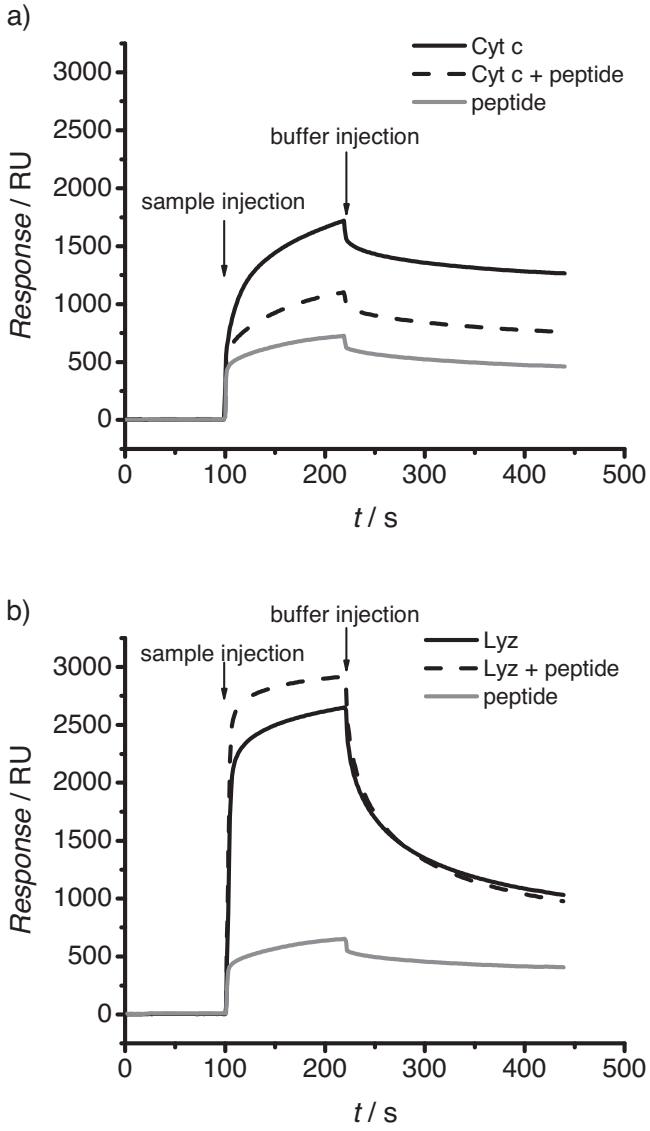

Figure 4. SPR sensorgrams in a competitive assay for the evaluation of selectivity of the imprinted film toward a) Cyt c and b) lysozyme in respect to the peptide template. The concentration of protein and peptide were kept constant at 50 μg mL^{-1} and 100 μg mL^{-1}, respectively.

Binding of Cyt c to the imprinted film was challenged by lysozyme (Lyz), bovine serum albumin (BSA), and myoglobin (Mb) as depicted in Figure 3b. At the same concentration of each protein, Cyt c revealed the highest SPR response followed by lysozyme, while BSA and Mb only gave very low responses. Unexpectedly, the response of lysozyme was relatively high as compared to Cyt c.

To confirm whether lysozyme shares the same binding site with the peptide or not, competitive binding experiment was performed. In contrast to Cyt c, the response of the mixture solution containing lysozyme and the peptide was even higher than the response of lysozyme alone (Figure 4b). The observed summation of the responses of both analytes indicates that the binding of lysozyme and the peptide to the imprinted film occurs at different sites. While the peptide binds specifically to the imprinted sites, lysozyme rather binds to the surface of the MIP film via non-specific interactions. It has been reported that lysozyme is one of the most surface active protein and it already exists in a dimer form in solution at the pH region from 5 to 10.[39–41] Previous experimental[42–44] and theoretical studies[45–47] have proved that driven by electrostatic forces and multiprotein interactions positively charged lysozyme can cluster, form multilayer, or aggregate on a charged solid surface primarily through its arginine rich surface. This was confirmed in our experiment where binding of lysozyme could not be observed after increasing the concentration of NaCl in the rebinding buffer to 1 M (data not shown). Since the charge interaction plays a key role in the aggregation mechanism, lysozyme would more efficiently cluster or aggregate on the more negatively charged MIP surface rather than the NIP surface. This would possibly explain the high SPR response of our MIP film for lysozyme.

3. Conclusions

We have demonstrated a new surface confined epitope imprinting approach to prepare a homogeneous ultrathin

film in an aqueous solution for selective protein recognition. In comparison to the work of Nishino et al. our strategy offers some attractive features especially its straightforward procedure which allows the MIP film to be directly prepared onto the transducer surface. There is no need to peel the MIP film off the substrate. Moreover, a fine control of the film thickness is maintained by the electrochemical deposition protocol. Our approach is by no means limited to a particular peptide template, target protein, or electropolymer. Various electropolymerizable materials like pyrrole, thiophene derivatives (with and without additives) or co-polymers can be used to improve the affinity of the imprinted film. Last but not least, our approach is versatile and can be applied to various gold based sensor platforms involving electrochemical, acoustic, and optical sensors.

4. Experimental Section

Materials: Gold coated disks 1 inch in diameter with 200 nm gold layer thickness and SPR sensor chips were purchased from Ssens (Netherlands). Scopoletin, cytochrome c (Cyt c) from bovine heart, myoglobin (Mb) from equine heart, lysozyme (Lyz) from chicken egg white, bovine serum albumin (BSA), and all other chemicals were purchased from Sigma-Aldrich (Germany) and were of analytical grade or higher. Dy-633-NHS-ester was purchased from Dyomics GmbH (Germany). Cysteine-terminated TAMRA labeled peptide template (TAMRA-AYLKKATNEC) and other peptides (AYLKKATNE, AYLAKATNE, AYLKKITNE, PFYYVPDYASGS, DVFYPYPYASGS) used were purchased from Centic Biotec (Germany). Dy-633 labeled peptide (C(Dy-633-M)-AYLKKATNE) was purchased from Biosyntan (Germany). All buffer salts were purchased from Roth (Germany). Ultrapure water from a laboratory water purification system (Sartorius, Germany) was used throughout this work.

Instrumentation: All electrochemical experiments were performed using an Autolab Potentiostat/Galvanostat PGSTAT30 interfaced with the General Purpose Electrochemical System (GPES) software (Eco Chemie, Netherlands). A three-electrode system with a thin-film gold disk, a Pt wire counter electrode, and an Ag/AgCl (1M KCl) reference electrode was used. Fluorescence imaging was performed using a Tecan LS Reloaded microarray scanner (TECAN GmbH, Germany) and the mean fluorescence intensity in arbitrary units for the selected area was calculated automatically by using Array-Pro Analyzer software. To make comparison possible from sample to sample, the scanner settings including scan area, exposure time, and gain were kept constant for all the measurements. Film thickness determination was conducted with a multimode ellipsometer (Multiskop, Optrel GmbH, Germany). The sample was placed on the sample holder, aligned perpendicular to the incidence plane of the laser beam (and the reflected laser beam) and illuminated with the 633 nm argon ion laser (1 mW). The reflected beam was detected by a 4-segment photodiode. By varying the incidence angle, the reflection minimum, associated with the surface plasmon resonance, was found. The thickness of the film was calculated from the minimum angle using the known index of refraction for poly-scopoletin ($n = 1.46$) with the help of the software included with the instrument. All the real-time, label-free rebinding experiments were performed using a Biacore T100 (GE Healthcare Bio-Sciences AB, Sweden) operated with Biacore T100 Control Software. Biacore T100 Evaluation Software was used to analyze the data obtained. Zeta potential measurement was done by using Electrokinetic Analyzer for Solid Surface Analysis: SurPASS (Anton Paar GmbH, Austria). AFM images were taken with a Nanowizard 3 BioScience AFM instrument (JPK instruments AG, Germany).

Peptide Template Immobilization: The clean gold chip was incubated in 0.05 mM cysteine-terminated Tamra-labeled peptide template in a freshly prepared 100 mM phosphate buffer (pH 7.4) containing 5 mM TCEP•HCl at 25 °C for 3 h. After 3 h, the gold chip was rinsed with water, agitated in 0.1% Tween-20 in PBS for 20 min, thoroughly rinsed with water, gently dried under N_2 flow, and stored in the dark until fluorescence imaging. The adsorption kinetics of the peptide template on the gold surface was investigated by varying the incubation time from 1 to 24 h. The concentration dependent adsorption was performed by keeping the incubation time constant at 3 h, while varying the concentrations of the peptide template from 0.01 to 1 mM.

Electropolymerization: An aqueous solution of 0.25 mM scopoletin and 20 mM EDTA in 100 mM NaCl was freshly prepared. Electropolymerization was conducted using a single potential pulse (0.7 V for 5 s, then 0 V for 15 s) without prior deoxygenation of the solution. After electrodeposition, the gold chip was rinsed with water, gently dried under N_2 flow, and stored in the dark until fluorescence imaging.

Template Removal: The peptide template was removed by electrochemical oxidation of the thiol by holding a potential pulse at 1.4 V for 30 s in a phosphate buffer solution (100 mM, pH 7.40). The gold chip was thoroughly rinsed by water and gently agitated in PBS buffer containing 0.1% Tween-20 overnight. Afterwards, the gold chip was rinsed with water, gently dried under N_2 flow, and stored in the dark until fluorescence imaging.

Preparation of Non-Imprinted Films: Non-imprinted control films were prepared in an identical manner as those performed in the preparation of the imprinted films, but in the absence of the peptide template on bare gold surfaces.

Batch Rebinding Studies: The gold chips with the imprinted or non-imprinted film were incubated for 18 h in a solution of the Dy633-labeled peptide (over the range of 1 to 75 μg mL^{-1}) or in a solution of Dy633-labeled Cyt c (over the range of 1 to 500 μg mL^{-1}). Labeling of Cyt c was done by using a standard protocol provided by Dyomics. All solutions were prepared in 0.1 M phosphate buffer (pH 7.4). A 5 min rinsing step with PBS containing 0.1% Tween-20 was employed to remove unspecifically bound peptide or protein. Afterwards, the chip was thoroughly rinsed with water, gently dried under N_2, and stored in the dark until fluorescence imaging.

Real-Time Rebinding Studies Using SPR: All measurements were performed in phosphate buffered saline tween 20 (PBST) of pH 7.4 with a flow rate of 30 μL min^{-1} at 25 °C. For each measurement, the buffer was first injected for 100 s to attain a stable baseline and to reach equilibrium. Cyt c, BSA, Mb, Lyz, template peptide (AYLKKATNE), and other control peptides (i.e., AYLAKATNE, AYLKKITNE, PFYYVPDYASGS, DVFYPYPYASGS) were used as the analytes to be investigated. The aqueous solutions of each peptide (100 μg mL^{-1}) and protein (50 μg mL^{-1}) were then injected for a contact time of 120 s. The buffer was subsequently injected for a dissociation time of 180 s. The report point, at which the binding response was assessed, was recorded at 270 s after the sample loading period. Selectivity of the imprinted film was verified by injecting peptides and proteins both in singular and in competitive manner.

Supporting Information

Supporting Information is available from the Wiley Online Library or from the author.

Acknowledgements

The authors gratefully acknowledge the financial support of BMBF (03IS2201A) of Germany. The authors also acknowledge Dr. Marion Frant and Dr. Holger Rothe (IBA GmbH, Heiligenstadt) for the Zeta potential and AFM measurements.

Received: May 16, 2012
Published online: August 3, 2012

[1] G. Wulff, W. Vesper, R. Grobe-Einsler, A. Sarhan, *Macromol. Chem. Phys.* **1977**, *178*, 2799–2816.
[2] K. J. Shea, E. A. Thompson, S. D. Pandey, P. S. Beauchamp, *J. Am. Chem. Soc.* **1980**, *102*, 3149–3155.
[3] R. Arshady, K. Mosbach, *Macromol. Chem. Phys.* **1981**, *182*, 687–692.
[4] C. Alexander, H. S. Andersson, L. I. Andersson, R. J. Ansell, N. Kirsch, I. A. Nicholls, J. O'Mahony, M. J. Whitcombe, *J. Mol. Recognit.* **2006**, *19*, 106–180.
[5] N. W. Turner, C. W. Jeans, K. R. Brain, C. J. Allender, V. Hlady, D. W. Britt, *Biotechnol. Prog.* **2006**, *22*, 1474–1489.
[6] A. Bossi, F. Bonini, A. P. F. Turner, S. A. Piletsky, *Biosens. Bioelectron.* **2007**, *22*, 1131–1137.
[7] D. E. Hansen, *Biomaterials* **2007**, *28*, 4178–4191.
[8] D. S. Janiak, P. Kofinas, *Anal. Bioanal. Chem.* **2007**, *389*, 399–404.
[9] N. M. Bergmann, N. A. Peppas, *Prog. Polym. Sci.* **2008**, *33*, 271–288.
[10] T. Takeuchi, T. Hishiya, *Org. Biomol. Chem.* **2008**, *6*, 2459–2467.
[11] Y. Ge, A. P. F. Turner, *Trends Biotechnol.* **2008**, *26*, 218–224.
[12] M. J. Whitcombe, I. Chianella, L. Larcombe, S. A. Piletsky, J. Noble, R. Porter, A. Horgan, *Chem. Soc. Rev.* **2011**, *40*, 1547–1571.
[13] A. V. Linares, F. Vandevelde, J. Pantigny, A. Falcimaigne-Cordin, K. Haupt, *Adv. Funct. Mater.* **2009**, *19*, 1299–1303.
[14] A. Bossi, C. Rivetti, L. Mangiarotti, M. J. Whitcombe, A. P. F. Turner, S. A. Piletsky, *Biosens. Bioelectron.* **2007**, *23*, 290–294.
[15] O. Hayden, P. A. Lieberzeit, D. Blaas, F. L. Dickert, *Adv. Funct. Mater.* **2006**, *16*, 1269–1278.
[16] A. Menaker, V. Syritski, J. Reut, A. Öpik, V. Horváth, R. E. Gyurcsányi, *Adv. Mater.* **2009**, *21*, 2271–2275.
[17] A. Nematollahzadeh, W. Sun, C. S. A. Aureliano, D. Lütkemeyer, J. Stute, M. J. Abdekhodaie, A. Shojaei, B. Sellergren, *Angew. Chem.* **2011**, *123*, 515–518; *Angew. Chem. Int. Ed.* **2011**, *50*, 495–498.
[18] G. Lautner, J. Kaev, J. Reut, A. Öpik, J. Rappich, V. Syritski, R. E. Gyurcsányi, *Adv. Funct. Mater.* **2011**, *21*, 591–597.
[19] A. Rachkov, N. Minoura, *J. Chromatogr. A* **2000**, *889*, 111–118.
[20] D. F. Tai, C. Y. Lin, T. Z. Wu, L. K. Chen, *Anal. Chem.* **2005**, *77*, 5140–5143.
[21] D. F. Tai, M. H. Jhang, G. Y. Chen, S. C. Wang, K. H. Lu, Y. D. Lee, H. T. Liu, *Anal. Chem.* **2010**, *82*, 2290–2293.
[22] G. Ertürk, L. Uzun, M. A. Tümer, R. Say, A. Denizli, *Biosens. Bioelectron.* **2011**, *28*, 97–104.
[23] C. H. Lu, Y. Zhang, S. F. Tang, Z. B. Fang, H. H. Yang, X. Chen, G. N. Chen, *Biosens. Bioelectron.* **2012**, *31*, 439–444.
[24] H. Nishino, C. S. Huang, K. J. Shea, *Angew. Chem.* **2006**, *118*, 2452–2456; *Angew. Chem. Int. Ed.* **2006**, *45*, 2392–2396.
[25] D. M. Hawkins, A. Trache, E. A. Ellis, D. Stevenson, A. Holzenburg, G. A. Meininger, S. M. Reddy, *Biomacromolecules* **2006**, *7*, 2560–2564.
[26] M. Zayats, M. Kanwar, M. Ostermeier, P. C. Searson, *Macromolecules* **2011**, *44*, 3966–3972.
[27] C. Malitesta, E. Mazzotta, R. A. Picca, A. Poma, I. Chianella, S. A. Piletsky, *Anal. Bioanal. Chem.* **2012**, *402*, 1827–1846.
[28] P. S. Sharma, A. Pietrzyk-Le, F. D'Souza, W. Kutner, *Anal. Bioanal. Chem.* **2012**, *402*, 3177–3204.
[29] N. Luo, D. W.Hatchett, K. R. Rogers, *Electroanalysis* **2007**, *19*, 2117–2124.
[30] T. Takeuchi, T. Hishiya, *Org. Biomol. Chem.* **2008**, *6*, 2459–2467.
[31] N. Gajovic-Eichelmann, E. Ehrentreich-Förster, F. F. Bier, *Biosens. Bioelectron.* **2003**, *19*, 417–422.
[32] Y. Chen, J. Yang, Z. Wang, X. Wu, F. Wang, *Spectrochim. Acta A* **2007**, *66*, 686–690.
[33] W. Schuhman, C. Kranz, H. Wohlschlager, J. Strohmeier, *Biosens. Bioelectron.* **1997**, *12*, 1157–1167.
[34] M. Komiyama, T. Takeuchi, T. Mukawa, H. Asanuma, *Molecular Imprinting*, Wiley-VCH, Weinheim **2003**, pp. 50–52
[35] G. Scatchard, *Ann. N. Y. Acad. Sci.* **1949**, *51*, 660–672.
[36] S. Hirota, Y. Hattori, S. Nagao, M. Taketa, H. Komori, H. Kamikubo, Z. Wang, I. Takahashi, S. Negi, Y. Sugiura, M. Kataoka, Y. Higuchi, *Proc. Natl. Acad. Sci. USA* **2010**, *107*, 12854–12859.
[37] J. Hanske, J. R. Toffey, A. M. Morenz, A. J. Bonilla, K. H. Schiavoni, E. V. Pletneva, *Proc. Natl. Acad. Sci. USA* **2012**, *109*, 125–130.
[38] P. Weinkam, E. V. Pletneva, H. B. Gray, J. R. Winkler, P. G. Wolynes, *Proc. Natl. Acad. Sci. USA* **2009**, *106*, 1796–1801.
[39] A. J. Sophianopoulos, K. E. Van Holde, *J. Biol. Chem.* **1964**, *2391*, 2516–2524.
[40] M. R. Bruzzesi, E. Chiancone, E. Antonini, *Biochemistry* **1965**, *4*, 1796–1800.
[41] O. G. Hampe, C. V. Tondo, A. Hasson-Voloch, *Biophys. J.* **1982**, *40*, 77–82.
[42] D. T. Kim, H. W. Blanch, C. J. Radke, *Langmuir* **2002**, *18*, 5841–5850.
[43] D. Pellenc, R. A. Bennett, R. J. Green, M. Sperrin, P. A. Mulheran, *Langmuir* **2008**, *24*, 9648–9655.
[44] T. Wei, S. Kaewtathip, K. Shing, *J. Phys. Chem. C* **2009**, *113*, 2053–2062.
[45] K. Kubiak, P. A. Mulheran, *J. Phys. Chem. B* **2009**, *113*, 12189–12200.
[46] K. Kubiak-Ossowska, P. A. Mulheran, *Langmuir* **2010**, *26*, 15954–15965.
[47] K. Kubiak-Ossowska, P. A. Mulheran, *J. Phys. Chem. B* **2011**, *115*, 8891–8900.